

Simulation and scale-up of the desulphurization of gas streams by adsorption method using numerical simulation

João Paulo Lobo dos Santos^{a,*}, Ana Katerine de Carvalho Lima Lobato^b, Caetano Moraes^c,
Acto de Lima Cunha^a, José Jailton Marques^d, Luiz Carlos Lobato dos Santos^e

^a Federal University of Sergipe - Petroleum Engineering Core - Av. Marechal Rondon, s/n - Jardim Rosa Elze, CEP: 49100-000, São Cristóvão, SE, Brazil

^b School of Exact and Technological Sciences, Salvador University, R. Dr. José Peroba, 251-Stiep, CEP 41770-235, Salvador, BA, Brazil

^c Federal University of Rio de Janeiro, Department of Chemical Engineering, Av. Horácio Macedo, 2030, Ilha do Fundão, CEP 21941-909, Rio de Janeiro, RJ, Brazil

^d Federal University of Sergipe, Department of Environmental Engineering, Av. Marechal Rondon, s/n - Jardim Rosa Elze, CEP: 49100-000, São Cristóvão, SE, Brazil

^e Federal University of Bahia, Postgraduate Program of Chemical Engineering, R. Prof. Aristides Novis, 2, 2^o andar, Federação, CEP 40210-630, Salvador, BA, Brazil

ARTICLE INFO

Keywords:

Natural gas
Hydrogen sulfide
Adsorption
Scale-up
Simulation

ABSTRACT

Natural Gas usually contains H₂S as a major contaminant, and its presence in gas streams can lead to corrosion of equipment and pipelines. Adsorption is a commonly used technique for removing sulfur compounds from gas streams at low concentrations. The desulphurization process is very complex, requiring experimental and pilot-scale studies before the development of a full-scale adsorption column. Such studies often involve simulation and scale-up techniques. Approaches for scale-up techniques applied to the removal of H₂S from natural gas in real conditions of transport lacks discussions in the literature. The present study aimed to perform a scale-up of experimental pilot-scale equilibrium data for the real conditions of natural gas transport through gas pipelines using numerical simulation. We evaluated the influence of operating parameters (bed length/diameter ratio, pressure, and temperature) on the removal of H₂S from a gas stream in the range of 1.5–3.5, 50–110 bar, and 298–328 K, respectively. The predicted results match real process data providing the elaboration of a scale-up for gas transport conditions in a pipeline. The results showed that at the confidence level of 95%, only pressure was statistically significant, and the optimization of operating conditions increased the amount adsorbed in the equilibrium from 3.71 to 4.70 mol/kg. Bed saturation time was estimated for different operating flows, and the results are in agreement with data reported in the literature.

1. Introduction

There has been an enormous growth in worldwide energy demands. At the same time, the need for sustainable policies has become mandatory since the ratification of Kyoto's Protocol. In this scenario, Natural Gas (NG) stands out as an energy source with numerous environmental benefits, such as low sulfur dioxide, nitrogen oxides, particulate matter, and carbon dioxide emissions (Santos et al., 2015). NG represents 23.7% of global primary energy consumption, with a 1.6% annual growth, and more than 80% of this demand comes from the industrial and energy sectors (Faramawy et al., 2016).

Natural gas often contains H₂S and CO₂ as major impurities, and the removal of these compounds becomes paramount to the chemical industry (Mirfendereski and Mohammadi, 2017; Rezakazemi et al., 2011).

H₂S is a highly toxic and corrosive gas (Faiz and Al-Marzouqi, 2010; Teles and Silva, 2015), and its combustion contribute to sulfur dioxide emissions, which have harmful environmental effects (Zulkefli et al., 2017). The presence of H₂S in gas streams can lead to the deactivation of metal-metal oxide catalysts in some processes. It can also cause the corrosion of equipment and pipelines (Melo et al., 2006; Zulkefli et al., 2017). Moreover, H₂S may be the source of elemental sulfur formation (S₈) (Kimtantis and Taylor, 2014) or even act as a solvent by increasing the ability of natural gas to carry S₈ (Pack et al., 2012), causing the formation of deposits in pipelines, which in turn cause blockages (Zhou et al., 2013). Given the various problems presented, the removal of H₂S from gas streams is essential to upgrade quality, avoid any cost increment, and to provide a better environment (Zulkefli et al., 2017).

The removal of hydrogen sulfide from gas streams such as natural gas

* Corresponding author. Federal University of Sergipe, Petroleum Engineering Core, Av. Marechal Rondon, s/n - Jardim Rosa Elze, CEP: 49100-000, São Cristóvão, SE, Brazil.

E-mail address: jplobo2011@gmail.com (J.P. Lobo dos Santos).

<https://doi.org/10.1016/j.jngse.2020.103693>

Received 17 June 2020; Received in revised form 21 September 2020; Accepted 23 October 2020

Available online 27 October 2020

1875-5100/© 2020 Elsevier B.V. All rights reserved.

belongs to an important area called hydrocarbon desulphurization (Oliveira et al., 2014). Thus, the desulphurization process of gas streams can be done by several technologies, such as biological, chemical absorption (extraction by amine solution), and adsorption by using mesoporous material and membrane-based gas permeation technologies (Oliveira et al., 2014; Zulkefli et al., 2019). Fixed bed adsorption is one of the most recommended techniques, both from the complexity and economic viewpoints (Santos et al., 2016; Coppola and Papurello, 2018). Several adsorbents can be used for this process. However, the literature highlight zeolites (Melo et al., 2006; Ryzhikov et al., 2011; Liu et al., 2016; Yousefi et al., 2017), activated carbon (Wang et al., 2015; Castrillon et al., 2016; Sigot et al., 2016a), metal oxides (Ratnasamy et al., 2012; Sekhavatjou et al., 2014) and silica (Ko et al., 2007; Watabe and Yogo, 2013). From the listed adsorption technologies, zeolites are already widespread and commercially available, and it can be used in large-scale processes such as gas transport pipelines for H₂S removal from natural gas.

The transportation of natural gas through pipelines, as well as its treatment, involves high flow rates and pressures, which impair the reproduction of real processes via laboratory experiments (Santos et al., 2018). Before setting up a full-scale adsorption column, experimental studies are usually done in small fixed bed size. Furthermore, pilot-scale experiments can be expensive and time-consuming (Svedberg, 1979). Thus, the scale-up methods allow the theoretical prediction of the adsorption column dynamics via numerical solutions of the differential equations governing the phenomenon. In this scenario, process simulators appear as efficient tools to solve this problem under various design conditions, also being an alternative for time and cost optimization toward results (Kim et al., 2012). Advances in numerical methods and computational power have been allowed to predicted fluid flow behavior, although of the use of numerical solution techniques. From the numerical analyses, fixed bed behavior can be widely studied for an extensive set of operating conditions in little time and cost.

The literature lacks discussions on approaches for scale-up techniques applied to the removal of H₂S from natural gas during transport. The main goal of this work is to develop a scale-up process based on the experimental data obtained from pilot-scale studies. In doing so, it is possible to predict the real conditions of natural gas transport in pipelines. The numerical solution technique was used to obtain the solution of the governing equations and to obtain a rupture curve for H₂S removal in a fixed bed column using zeolite 13× as adsorbent. The model predictions were validated against experimental data before performing a scale-up of the natural gas transport conditions, allowing the generation of breakthrough curves for high flows and pressures.

2. Materials and methods

2.1. Experimental pilot data

The simulation methodology was used according to our previous study, in which the Sips isotherm model was pointed out as the best choice to represent the equilibrium data for H₂S adsorption on zeolite 13× (Santos et al., 2018). Moreover, we checked if the equilibrium data by Sigot et al. (2016a) (Base Case 1) could be adjusted to predict the breakthrough curve presented by Melo et al. (2006) (Base Case 2), which was obtained for different feed gas composition and operating conditions, as shown in Table 1. In both studies, zeolite 13× was used as an adsorbent to evaluate if a scale-up based on the data for different operating conditions could be performed by adjusting the equilibrium data.

2.2. Process description

This process consists of adsorption columns operating in parallel, and it can be located in a platform with similar characteristics of Hasbah field (Alami et al., 2012). Cylindrical columns were filled with 13×

Table 1

Feed specifications and bed characteristics from experimental data.

Parameters	Base Case 1	Base Case 2
H ₂ S concentration in the feed (mol/m ³)	0.158	0.02
Bed length (m)	0.1	0.04
Bed diameter (m)	0.04	3.1x10 ⁻³
Particle diameter (m)	0.002	0.002
Particle density (kg/m ³)	1130	1130
Particle porosity [-]	0.24	0.24
Particle tortuosity	1.38	1.38
Average pore diameter (m)	7.4x10 ⁻¹⁰	7.4x10 ⁻¹⁰
Bed density (kg/m ³)	700	660
Bed porosity [-]	0.36	0.41
Feed rate (m ³ /s)	1.66 x10 ⁻⁵	5 x10 ⁻⁷
Temperature (K)	298	298
Manometric pressure (bar)	1	4.9

Source: Santos et al. (2019).

zeolite as adsorbents, and the height and diameter were optimized in the simulations. During operation, some beds are operating at high pressure to separate impurities like H₂S, while other beds could be in regeneration mode. The amount of bed operating in parallel can be determined from the bed saturation time.

In Hasbah field, in Saudi Arabia, a pipeline is used to transport gas from the production platform to an inland processing plant located 130 km away. The pipeline consists of a 36-inch (0.914 m) tube, transporting a flow rate of 1.3 million SCF/day, according to Alami et al. (2012). In this field, the problem of elemental sulfur formation and deposition occurs, requiring the removal of H₂S from the natural gas stream before transportation as an alternative to avoid the S₈ deposition. Thus, the installation of a desulphurization unit in the production platform would be of help. The gas stream pressure and the temperature in the wellhead are 1600 psia (110 bar) and 77 °F (298 K), respectively.

2.3. Governing equations

In order to understand the dynamic behavior of an adsorption bed, a mathematical model is needed to incorporate mass balance over a packed bed with appropriate boundary conditions. For this system, the following assumptions are introduced:

- ✓ Transient regime, isothermal and adiabatic flow (Khademi et al., 2015; Santos et al., 2018);
- ✓ Gas stream properties follow the Peng-Robinson state equation (Ahari et al., 2016);
- ✓ Temperature, pressure, and concentration gradients in radial and angular directions are neglected (the column is considered one-directional) (Ahari et al., 2016; Yousefi et al., 2017);
- ✓ The properties density, porosity, permeability, and interstitial velocity are considered constant along the bed (Santos et al., 2018);
- ✓ The mass transfer rate between the gas phase and the solid phase is represented by linear driving force (LDF) (Ahari et al., 2016; Yousefi et al., 2017);
- ✓ The mass transfer consists of the coefficients of film resistance and macropore diffusion (Khademi et al., 2015);
- ✓ Only physical adsorption was considered (Santos et al., 2018).

According to these assumptions, the mass balance between gas and solid phase has been described by Equation (1) (Qazvine and Fatemi, 2015):

$$\frac{\partial C}{\partial t} = D_L \frac{\partial^2 C}{\partial z^2} - v \frac{\partial C}{\partial z} - \frac{(1 - \epsilon)\rho_p}{\epsilon} \frac{\partial q}{\partial t} \quad (1)$$

Where: D_L is the coefficient of axial dispersion, C is the concentration of the solute in the fluid phase, z is the length of the bed, v is the interstitial velocity of the fluid, t is the time, ϵ is the porosity of the bed, ρ_p is the

density of the adsorbent and q is the concentration of the solute in the solid phase (adsorbed).

The Linear Driving Force, which describes the mass transfer rate between the gas phase and the solid phase, is represented by Equation (2):

$$\frac{\partial q}{\partial t} = K_s(q_e - q) \quad (2)$$

Where: K_s is the global mass transfer coefficient, and q_e is the value of q in equilibrium with C .

In order to solve the mass balance described by Equations (1) and (2), we used the interface coefficient form PDE in Comsol Multiphysics, which numerically solve the differential equations using the variable u , as shown in Equation (3) (Aguilera and Ortiz, 2016):

$$e_a \frac{\partial^2 u}{\partial t^2} + d_a \frac{\partial u}{\partial t} + \nabla(-c \nabla u - au + \gamma) + \beta \nabla u + au = f \quad (3)$$

Where: e_a is the mass coefficient, d_a is the damping or mass coefficient, c is the diffusion coefficient, a is the conservative flow convection coefficient, γ is the conservative flow source term, β is the convection coefficient, a is the sorption coefficient, and f is the source term.

In order to be able to use the coefficient form PDE, which is dependent on time and one-dimensional flow, it is necessary to make Eqs. (1) and (2) dimensionless for concentration, adsorbed amount, time, and length. For this, we used dimensionless variables u_1 , u_2 , l , and τ , as described by Equations (4)–(7):

$$u_1 = \frac{C}{C_0} \quad (4)$$

$$u_2 = \frac{q}{q_0} \quad (5)$$

$$\tau = \frac{tv}{L} \quad (6)$$

$$l = \frac{z}{L} \quad (7)$$

Where: u_1 is the dimensionless concentration of H_2S in the gas phase, u_2 is the dimensionless concentration of H_2S in the solid phase, τ is the dimensionless time, v is the interstitial velocity, l is the dimensionless length, and L is the length of the bed.

Replacing Equations (4)–(7) in Equations (1) and (2) and then Equation (2) in Equation (1), after some mathematical simplifications, the dimensionless equation that describes the mass balance in the bed is described by (8):

$$\frac{\partial u_1}{\partial \tau} = \frac{D_L}{Lv} \frac{\partial^2 u_1}{\partial l^2} - \frac{\partial u_1}{\partial l} - \frac{(1-\epsilon)\rho_p q_0}{\epsilon C_0} \frac{k_s L}{v} (u_2^* - u_2) \quad (8)$$

Where: u_2^* corresponds to the isothermal models described in this work by the Sips model.

From Equation (8), it is possible to obtain some dimensionless variables that will be implemented in the PDE coefficient form, as can be seen from Equations (9)–(11):

$$P_e = \frac{vL}{D_L} \quad (9)$$

$$D_g = \frac{(1-\epsilon)\rho_p q_0}{\epsilon C_0} \quad (10)$$

$$S = \frac{k_s L}{v} \quad (11)$$

Where: P_e is the Peclet number, D_g is called the distribution coefficient, and S is the dimensionless global mass transfer coefficient.

Comparing Equations (3) and (8), the implementation of the

coefficients in the PDE coefficient form is as follow: $e_a = (0)$, $d_a = (D_g)$, $c = \left(\frac{1}{P_e}\right)$, $\alpha = (-1)$, $\gamma = (0)$, $\beta = (0)$, $a = (S)$ and $f = (u_2^*)$.

It is necessary to determine the axial dispersion coefficient and the dimensionless global mass transfer coefficient to implement the coefficients of Equations (9) and (11). The axial dispersion coefficient was determined by Equation (12) (Dantas et al., 2011):

$$\frac{\epsilon D_L}{D_m} = 0.23 + 0.5ScRe \quad (12)$$

Where: Sc is the Schmidt number, Re is the Reynolds number, and D_m is the molecular diffusivity.

The Reynolds number describes the ratio between the inertial and viscous forces, while the Schmidt number is defined as the ratio of the moment diffusivity and mass diffusivity, which can be determined by Equations (13) and (14), respectively (Aguilera and Ortiz, 2016):

$$Re = \frac{\rho u d_p}{\epsilon \mu} \quad (13)$$

$$Sc = \frac{\mu}{\rho D_m} \quad (14)$$

Where: ρ is the gas specific mass, u is the surface velocity of the gas, d_p is the diameter of the adsorbent particle, and μ it is the viscosity of the gas.

The Fuller-Schettler-Gridding correlation was used to obtain the molecular diffusivity, according to Equation (15) (Ortiz et al., 2014):

$$D_m = \frac{10^{-3} T^{1.75} \left(\frac{1}{MM_{gas}} + \frac{1}{MM_{H_2S}} \right)^{0.5}}{P \left(V_{gas}^{1/3} + V_{H_2S}^{1/3} \right)^2} \quad (15)$$

Where: T is the temperature, MM_{gas} is the molecular mass of the gas, MM_{H_2S} is the molecular mass of H_2S , P is the pressure, V_{gas} is the diffusion volume of the gas, and V_{H_2S} is the diffusion volume of H_2S . It was assumed dimensionless values of 24.42 and 20.96 for the diffusion volume of methane and H_2S , respectively.

In order to determine the mass transfer coefficient, it was assumed the film resistance and macropore diffusion, as shown in Equation (16) (Aguilera and Ortiz, 2016):

$$\frac{1}{K_s} = \frac{d_p q_0 \rho_b}{6k_g c_0 \epsilon} + \frac{d_p^2 q_0 \rho_b}{60D_e c_0 \epsilon} \quad (16)$$

Where: q_0 is the value of q (concentration in the solid phase) in equilibrium, ρ_b is the density of the bed, k_g is the coefficient of external mass transport, C_0 is the contraction of H_2S in the supply, and D_e is the effective diffusivity.

The Wakao-Funazkri correlation was used to determine the external mass transfer coefficient, and it uses the Sherwood number (Sh), according to Equations (17) and (18) (Xu et al., 2013):

$$Sh = 2 + 1.1Sc^{1/3}Re^{0.6} \quad 3 < Re < 10000 \quad (17)$$

$$k_g = \frac{Sh D_m}{d_p} \quad (18)$$

The Bosanquet equation was used for calculation of the effective diffusivity in the macroporous, as Equation (19) (Khademi et al., 2015):

$$\frac{1}{D_e} = \tau_p \left[\frac{1}{D_m} + \frac{1}{D_K} \right] \quad (19)$$

Where: τ_p is the tortuosity factor of the particle, and D_K is the Knudsen diffusivity.

The Knudsen diffusivity and the tortuosity factor of the particle can be obtained from Equations (20) and (21) (Khademi et al., 2015):

$$D_K = 97r_{pore} \left(\frac{T}{MM_{H_2S}} \right)^{0.5} \quad (20)$$

$$\tau_p = \varepsilon_p + 1.5(1 - \varepsilon_p) \quad (21)$$

Where: r_{pore} is the radius of the pore, T is the temperature, and ε_p is the porosity of the particle.

2.3.1. Boundaries and initial conditions

For a numerical solution of the problem, it is necessary to define the boundary and initial conditions and, in this case, they are described by Equation (22):

$$\begin{aligned} \tau = 0, u_1 = 0, u_2 = 0 \quad (0 \leq l \leq 1) \\ l = 0, u_1 = 1, (\tau > 0) \\ l = 1, \frac{\partial u_1}{\partial l} = 0, (\tau > 0) \end{aligned} \quad (22)$$

In order to describe the conditions in Eq. (22) it is necessary to add two boundary conditions: Dirichlet type for $l = 0$ ($u = r$) and Flux-Source type for $l = 1$ ($-n(-c\nabla u - au + \gamma) = g - q_a u$). For the coefficient form PDE interface, the boundary conditions are described by: $r = (1)$, $q_a = (1)$ and $g = (0)$.

The amount of H_2S adsorbed by the adsorption column is a function of concentration, pressure, and temperature as follows: $q = f(C_o, P, T)$. Thus, for the operating conditions that take into account the installation of the adsorption unit in the Hasbah field facility, the amount of adsorbate adsorbed at equilibrium can be predicted through Equation (23) (Santos et al., 2019):

$$C = \frac{P \cdot y_i}{R \cdot T} \quad (23)$$

Where: P is the pressure (bar), y_i is the molar fraction of adsorbate in the mixture (ppmv/ 10^6), R is the universal gas constant ($83.14 \times 10^{-6} \text{ m}^3 \cdot \text{bar/mol.K}$), and T is the temperature (K).

The value obtained from Eq. (23) was used by the Sips isotherm model to predict the adsorbed amount at equilibrium for a new desired concentration, pressure, or temperature condition in the adsorption unit, according to Equation (24) e (25) (Santos et al., 2019).

$$q_e = \frac{q_m \cdot (b_s \cdot C)^{1/n}}{1 + (b_s \cdot C)^{1/n}} \quad (24)$$

$$b_s = b_0 \cdot e^{\left(\frac{-\Delta H}{RT} \right)} \quad (25)$$

Where: q_m is the maximum adsorbed amount at equilibrium (mol/kg), b_s and n are constants of the Sips model, b_0 is the adsorption constant at infinite temperature, and ΔH is the adsorption heat assuming 35.5 kJ/mol according to Wynnyk et al. (2017).

2.3.2. Solution for model equations

In order to solve the mentioned set of second and first-order partial differential equations for each step of the adsorption process, they have to be discretized using the Finite Element Method using Comsol Multiphysics. In this software, to solve the partial differential equations, it uses the interface coefficient form PDE. In the present study, to run simulations, the bed length has been divided using a mesh with 5000 triangular elements, a dimensionless time step of 10, and a relative tolerance equal to 10^{-6} .

2.4. Statistical evaluation of the influence of operating parameters

In order to maintain the geometric similarity between the pilot-scale adsorption column and the full-scale adsorption bed to be installed

offshore, the bed dimensions were estimated by considering a scale factor of 30 concerning the values by Sigot et al. (2016a). These values are in the same order of magnitude as the system proposed by Anerousis and Whitman (1985), applied to the H_2S removal by adsorption on activated carbon. By guaranteeing that the new values for dimensionless transport numbers remained within the range for which correlations are valid, the existence of dynamic similarity was verified.

A constant gas flow production of 1.3 million SCF/day ($0.420 \text{ m}^3/\text{s}$) was considered in order to optimize the bed design in the scale-up for the Hasbah field, as well as its operating parameters. A parametric analysis was carried out, systematically changing the following parameters: bed length/diameter ratio (L/D), pressure in the adsorption column (P), and adsorption temperature (T). An experimental design was carried out using a fractional factorial design, resulting in a total of 9 simulations. The values of the operational variables were coded as (-1) for lower levels, (0) for the central level, and (+1) for upper levels, as shown in Table 2.

The bed length and diameter used in each L/D ratio were 2.17 m and 1.44 m, 3.05 m and 1.22 m, and 3.82 m and 1.09 m, respectively. As a result, the bed volume and, consequently, the adsorbent mass were kept constant for all situations and, thus, it does not change from one simulated case to another. To statistically evaluate the results, we used the amount of H_2S adsorbed until bed exhaustion, using the Statistica 8.0 software. The variables were assessed at a 95% confidence level. From the results, it was possible to obtain the significance of the variables through the Pareto chart, response surface, and Analysis of Variance (ANOVA), which provides a mathematical model predictive for the investigated parameter. Also, it was possible to check if there is an interaction between the evaluated effects and, thus, seek an optimization for the operating conditions of the adsorption bed.

As seen in Table 2, breakthrough curves were simulated using different L/D ratios, and the influence of this parameter on the bed dynamics was evaluated. For all flow rates evaluated, the dimensionless transport numbers used were verified, ensuring that they remained within the range of values from which the employed correlations were obtained.

Moreover, a study on the optimal operating conditions for the gas pipeline was performed according to Vijayaraghavan et al. (2005), who reported that the increase in flow rates results in the reduction of mass transfer resistance. From a certain point on, this effect is no longer significant and, therefore, an optimum workflow can be determined for the bed operation. Thus, the increase in flow rates allows the decrease in length of the Mass Transfer Zone (MTZ) to the optimum flow and, consequently, the MTZ length increases again. The MTZ size can be determined based on the operation time (t_u) and the saturation time (t_s), according to Equation (26) (Geankoplis, 1993):

$$MTZ = \left(1 - \frac{t_u}{t_s} \right) L \quad (26)$$

where: L is the length of the adsorption bed.

The useful time and the bed exhaustion time are determined by Equations (27) and (28), respectively.

$$t_u = \int_0^{t_p} \left(1 - \frac{C}{C_0} \right) dt \quad (27)$$

Table 2
Variables of fractional factorial design.

Factors	Levels		
	(-1)	(0)	(+1)
Bed length/diameter ratio (L/D)	1.5	2.5	3.5
Adsorption column pressure (bar)	50	80	110
Adsorption column temperature (K)	298	313	328

$$t_t = \int_0^{\infty} \left(1 - \frac{C}{C_0}\right) dt \quad (28)$$

Where: C_0 is the concentration of H_2S in feed, and t_b corresponds to the breakpoint time. The breakpoint and the exhaustion point are generally assumed at 5% and 95% of the outlet feed concentration (Possa et al., 2018).

By knowing the useful time and the exhaustion time, it is possible to estimate the useful capacity of the bed before rupture (q_u) and the point at which the saturation (q_{sat}) is reached through Equations (29) and (30), respectively:

$$q_u = \frac{C_0 Q}{m_{ads}} \int_0^{t_b} \left(1 - \frac{C}{C_0}\right) dt \quad (29)$$

$$q_{sat} = \frac{C_0 Q}{m_{ads}} \int_0^{\infty} \left(1 - \frac{C}{C_0}\right) dt \quad (30)$$

where: Q is the feed rate and m_{ads} is the adsorbent mass.

3. Results and discussions

3.1. Validation

Using Equation (23) and the experimental data from Sigot et al. (2016a), the equilibrium parameters were obtained as follows: $q_m = 12.9$ mol/kg, $b_s = 0.0142$ m³/mol and $n = 8.26$. Also, assuming heat of adsorption equals to 35.5 kJ/mol, the adsorption constant for infinite temperature was 8.5×10^{-9} m³/mol. The operating conditions of the adsorption bed may vary greatly depending on the case. Therefore, we verified whether we could represent the breakthrough curve obtained by Melo et al. (2006), based on the equilibrium data obtained from Sigot et al. (2016a), by adjusting only the pressure and concentration conditions - since the temperature was equivalent. Based on the Sips isotherm model, defined in our previous study as the one that best represented the experimental rupture curve, the breakthrough curves for experimental data of Sigot et al. (2016a), and Melo et al. (2006), were predicted, as shown in Fig. 1.

From Fig. 1, it can be seen that the modeling was able to satisfactorily predict both the experimental data by Sigot et al. (2016a) (B.C.1) and Melo et al. (2006) (B.C. 2). The B.C. 2 was obtained from the equilibrium data from the experimental study by Sigot et al. (2016a) and adjusted for the conditions of the adsorption bed of Melo et al. (2006). Therefore, it can be concluded that the correction of the equilibrium data obtained

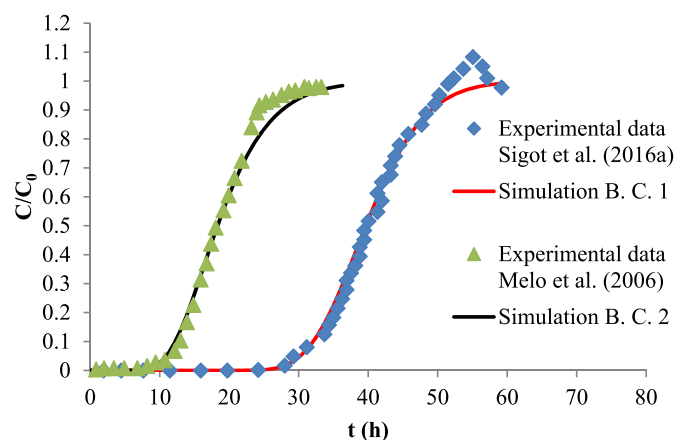


Fig. 1. Comparison between experimental and simulated breakthrough curves (B.C. refer to Base Case).

under different conditions can satisfactorily predict the breakthrough curve, as shown in the comparison between the experimental data by Melo et al. (2006) and the breakthrough curve shown in the simulation (B.C. 2). The errors do not exceed 5%, which shows a good prediction of the breakthrough curve. These results show the feasibility of scale-up techniques applied to the removal of H_2S from gas streams in different operating conditions. Table 3 shows the comparison between the adsorption and mass transfer parameters calculated by the adjusted Sips model and those obtained from the experimental data by Melo et al. (2006).

In Table 3, it is possible to see that the parameters calculated using the adjusted Sips isotherm model, and the values obtained from the experimental data are very close. The value predicted by the Sips model at equilibrium was 3.49 mol/kg, while the value obtained from the experimental data by Melo et al. (2006) was 3.26 mol/kg. Therefore, the adjusted Sips model was able to predict the equilibrium data satisfactorily and mass transfer parameters for different operating conditions since, in this case, the relative error between experimental and predicted values did not exceed 7%. According to Qazvine and Fatemi (2015), for relative errors of up to 10%, the simulated results are in agreement with real-world data. Thus, even for a different supply current composition, as well as for different concentrations and pressure conditions, the amount adsorbed at equilibrium could be satisfactorily predicted using the adjusted Sips isotherm model. The proposed methodology allows the application of the equilibrium data, with suitable corrections, to simulate higher pressure conditions. This allows a scale-up to the gas pipeline operating conditions and supplies the lack of experimental data taking into account the real transport conditions of natural gas.

3.2. Scale-up for natural gas transport conditions

The operating conditions for natural gas transport over a pipeline are often different from those under which pilot-scale experimental data are obtained. However, we were able to confirm the possibility of correcting the equilibrium data from one condition to another. So, the behavior of the desulphurization by adsorption can be evaluated when the flow, pressure, and temperature conditions that characterize a real gas pipeline are present. With these considerations in mind, a scale-up of the data was performed, where the equilibrium constants obtained from Sigot et al. (2016a), by using the Sips isotherm model, were adjusted for pressure and temperature conditions of the gas in the Hasbah field, according to the procedure previously established by Melo et al. (2006). As aforementioned, a feed stream composed of methane and H_2S can have its behavior predicted from the biogas data used by Sigot et al. (2016a). Therefore, a more straightforward binary composition was adopted for a gas stream transported over the pipeline.

The performance of the adsorbent bed was investigated by varying bed length/diameter ratio, bed operating pressure, and temperature. From that, it was possible to determine the rupture point and the amount adsorbed until that point, as well as the exhaustion time, the total adsorbed amount, and the MTZ length for each case. Table 4 shows the experimental design and the responses obtained in each case.

From the responses obtained in the simulations shown in Table 4, it was possible to evaluate the effects related to the three factors studied and their interactions in the amount of H_2S adsorbed until bed exhaustion. From the results of Table 4, the Pareto chart was used to show the most significant variables affecting the amount adsorbed until exhaustion, as shown in Fig. 2.

According to Abduredha et al. (2020), the Pareto chart depends on

Table 3
Predicted and experimental parameters of adsorption and mass transfer.

Parameters	q_0 (mol/kg)	K_s (s ⁻¹)	S	D_g
Predicted (Sips)	3.49	3.99×10^{-6}	1.04×10^{-6}	2.81×10^{-5}
Experimental B. C. 2	3.26	4.27×10^{-6}	1.11×10^{-6}	2.63×10^{-5}

Table 4
Experimental design and responses for three variables.

Cases	L/ D	P (bar)	T (K)	t _u (h)	t _r (h)	q _u (mol/ kg)	q _{sat} (mol/ kg)	MTZ (m)
1	-1	-1	-1	30.04	35.20	3.89	4.20	0.321
2	-1	0	1	19.61	22.37	3.60	3.87	0.270
3	-1	1	0	15.69	17.61	4.25	4.48	0.239
4	0	-1	-1	29.70	33.92	3.49	3.71	0.379
5	0	0	1	19.48	22.16	3.83	4.07	0.369
6	0	1	0	14.66	16.67	4.17	4.43	0.368
7	1	-1	-1	30.36	34.08	3.73	3.95	0.418
8	1	0	1	19.96	22.39	4.13	4.36	0.416
9	1	1	0	14.93	16.74	4.24	4.47	0.414

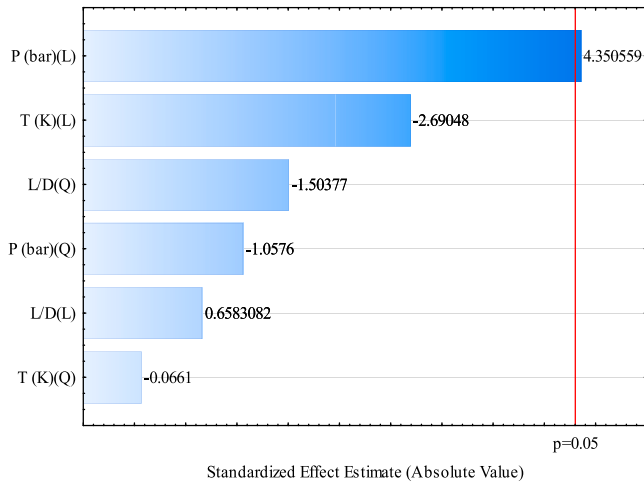


Fig. 2. Pareto chart for the evaluated variables.

the standard deviation results to estimate the sampling errors of variables, and an important sign is the p-value. From Fig. 2, the results were considered at a confidence level of 95%, and only the effect related to the variation of the linear adsorption pressure was statistically significant. From Table 4 and Fig. 2, it is possible to verify that the increase in pressure was the factor that most contributed to the increase in the adsorbed quantity. The increase in temperature, although not statistically significant for the evaluated levels, reduces the amount of H₂S adsorbed. Similar behavior had already been observed in previous studies, and this is because the adsorption is an exothermic process and follows Arrhenius' law (Santos et al., 2019). It is still possible to verify that for high pressures, the L/D ratios equal to 1.5 and 3.5 show values close to the adsorbed quantity and did not significantly influence the results obtained.

Table 4 also shows the dynamics of the bed based on the size of the MTZ. It is not possible to compare the length of the MTZ for all cases simulated together, because the MTZ depends on the length, as shown in Equation (26). However, MTZ length tends to remain constant at each length and diameter of the bed evaluated with the increase in the L/D ratio and indicates that the dispersion effects are being reduced. This behavior confirms that increasing Peclet number, the flow pattern is closer to the ideal plug flow. Through the statistical analysis of the results obtained, the values of the regression coefficients were found for the variables that describe the predictive empirical model, according to Equation (31).

$$q_{sat} = 3.994 + 0.038 \frac{L}{D} + 0.151 \left(\frac{L}{D} \right)^2 + 0.253P + 0.106P^2 - 0.156T + 0.00667T^2 \quad (31)$$

The presence of quadratic terms in Equation (31) obtained for the model confirms the statement that the dependence of the amount adsorbed on the factors evaluated is not linear. The quality of the model fit can be performed through ANOVA (Analysis of Variance) shown in Table 5.

Based on the data present in Table 5, for the significance level $\alpha = 0.05$, tabulated F (F_{tab}) and calculated F (F_{calc}) are equal to 5.14 and 14.99, respectively. Since F_{calc} > F_{tab}, it can be said that the model obtained has its approved statistical significance (Santos et al., 2019). Another important information in Table 5 is the adjusted R² value. Sometimes, the R² value tends to overestimate the impact of the factor(s) affecting response, and the adjusted R² is used to avoid what is referred to as overfitting (Ezeakacha and Salehi, 2019). According to Abdulredha et al. (2020) an R² value close to 1 indicates an acceptable goodness-of-fit of the models, and when an R² value is above 80% can be considered a good model. From the value of the adjusted R² (93.74%), a cautious conclusion can be made that the regression model shows high predictability of H₂S amount adsorbed in the exhaustion of the bed.

The response surface obtained for the evaluated factors ratifies that was observed in the previous analyzes, as can be seen in Fig. 3.

From Fig. 3a and b, it is possible to verify that keeping the temperature or the L/D ratio constant, the pressure effect is the one that most contributes to the increase of the adsorbed quantity. It is also possible to observe from the curvature of the response surface that the dependence of the amount adsorbed with the pressure is not entirely linear. Fig. 3b and c shows the linear effect of temperature on the adsorbed quantity, while in Fig. 3a and c, it is possible to verify in the evaluated intermediate L/D ratio the adsorbed quantity tends to decrease, being the most optimized condition for higher L/D ratios (case 9). This may be related to the increase in the Peclet number that varies from 898.9 to 1587.5 when the L/D ratio increases from 1.5 to 3.5. Therefore, the effects of the advective transport ratio are higher than the diffusion transport ratio, and so, if Peclet number increases the flow pattern is closer to ideal plug flow (Aguilera and Ortiz, 2016).

3.3. Operating rate effect

Considering the conditions of L/D ratio, pressure, and temperature that favors the increase of the amount adsorbed to the point of exhaustion, the optimum flow rate of the bed operation was evaluated by determining the MTZ size. Thus, simulations were carried out for the bed operating at a pressure of 110 bar, the temperature of 298 K and L/D ratio equal to 3.5 for different operating flow rates. The amount of H₂S adsorbed on the equilibrium was determined by the predictive model to be equal to 4.70 mol/kg. Fig. 4 shows the simulated breakthrough curves for different natural gas transport flows in the pipelines, considering the installation of the adsorption unit in the production platform in the Hasbah field.

Fig. 4 shows that an increase in the operating flow in the pipeline causes a shift of the breakthrough curve to the left, leading to earlier bed saturation. In addition, the slope is steeper due to the decrease in the axial dispersion coefficient, which increases the Peclet number and the increase in the overall mass transfer with the interstitial velocity, as seen in Table 6.

Table 6 reveals that even for an increase of almost twice in the external film mass transfer coefficient (k_g), the overall mass transfer

Table 5
ANOVA for the obtained model.

FV	SS	DF	MS	F _{calc}	F _{tab}	p-value
Regression	0.61	6	0.305	14.99	5.14	0.715
Residual	0.0407	2	0.0203			
Total	0.6507	8				

Note: Sum Squares (SS), Sum of Degrees of Freedom (DF), Sum of the Mean Squares (MS), for the regression: R² = 0.9374.

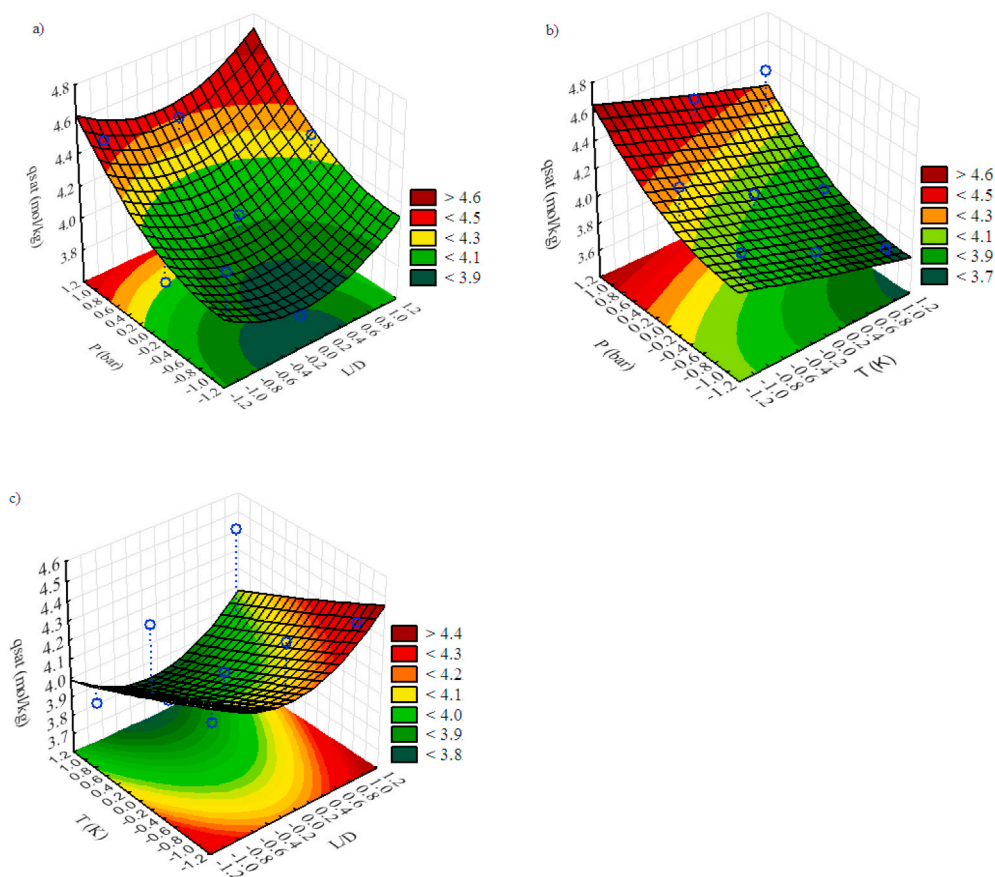


Fig. 3. Response surface as a function of: a) L/D ratio and pressure, b) pressure and temperature, and c) temperature and L/D ratio.

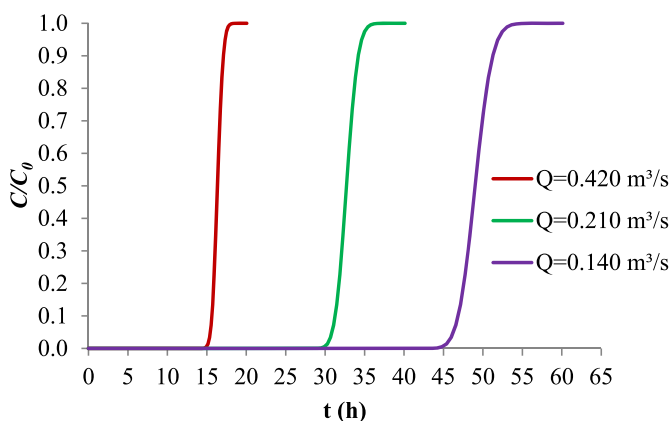


Fig. 4. Breakthrough curves for the gas pipeline operating in different flow rates.

Table 6
Mass transfer parameters under different operating flow rates.

Flow rates (m ³ /s)	k _g (m/s)	K _s (s ⁻¹)	S	D _g
0.140	0.0109	4.28x10 ⁻⁵	4.55x10 ⁻⁴	1.68x10 ⁴
0.210	0.0133	4.30x10 ⁻⁵	3.04x10 ⁻⁴	1.68x10 ⁴
0.420	0.0187	4.32x10 ⁻⁵	1.53x10 ⁻⁴	1.68x10 ⁴

coefficient (K_s) exhibits a tiny variation. According to Aguilera and Ortiz (2016), increasing velocity decreases breakpoint due to the reduction in residence time of molecules of H₂S with the adsorbent. This shows the fact that the global mass transfer coefficient is practically the same in the

three different flows, that the surface velocity is not very relevant, since the main resistance to mass transfer is due to the internal solid diffusion.

The increase in the flow rate increases the external mass transfer coefficient, while the overall mass transfer coefficient does not change in the same proportion. This happens because the H₂S adsorption in zeolite 13x is controlled by intraparticle diffusion and, due to the high flow rate, the shorter residence time is not sufficient to obtain high mass transfer rates, which makes MTZ, total and useable bed capacity practically independent on the flow variation, as shown in Table 7. Therefore, higher efficiencies require longer contact time. However, under natural gas transport conditions over pipelines, this is not always possible as high flow rates are involved, but higher residence time may be achieved by increasing the height of the column while keeping the interstitial velocity through the bed.

Despite the tiny difference, the smallest MTZ and the highest bed capacity occurred with the lowest flow rate. These results are in agreement with Ko et al. (2000), who stated that, in cases where the adsorption process is controlled by the resistance to mass transfer in the particle, low volumetric flow rates result in longer residence time, allowing the adsorption to occur, thus increasing the adsorption capacity. According to Geankoplis (1993), the lower the MTZ, the closer to ideality (step function) the system is, indicating less diffusion resistance. When $Pe \rightarrow \infty$, the case changes to plug flow when transport rate by diffusion can be neglected compared to the convection rate. It means

Table 7
Bed capacity and MTZ for different operating flow rates.

Flow rate (m ³ /s)	MTZ (m)	q _i (mol/kg)	q _{sat} (mol/kg)	Pe
0.140	0.414	4.395	4.636	1576.6
0.210	0.414	4.398	4.636	1582.0
0.420	0.415	4.399	4.632	1587.5

that, in this case, the quantity adsorbed does not show significant changes, since the intraparticle diffusion is the controlling step of the adsorption process. [Aguilera and Ortiz \(2014\)](#) concluded that axial dispersion could be neglected when the Peclet number exceeds 100.

Analyzing [Fig. 3](#) and [Table 7](#), one can conclude that the best scenario for the operation of the adsorption equipment is under the lowest flow conditions since, in this case, a more considerable saturation time is obtained. This is remarkable because, in the adsorption process, the adsorption capacity and the lifetime of the adsorbent are economically important factors, and under these conditions, these two parameters can be optimized. However, it is worthwhile to analyze if it is economically feasible to operate the adsorption column at the lowest flow rate. Since the velocity has a direct impact on the dynamics of the curves, and consequently on the residence time, an interstitial velocity of 0.361 m/s, which corresponds to the conditions of the lowest flow, could be kept, but a larger bed quantity should be used. In this case, for the entire Hasbah field, to treat the gas stream in the offshore production platform at a surface velocity of 0.361 m/s, three beds with 1.09 m diameter, and 3.82 m of length would be required. Besides, the required amount of adsorbent is three times higher, but the rupture time is also three times higher (46.3 h) and, therefore, the benefit-cost ratio could be compensated. This way, to operating with a parallel column, three beds could be on-stream at high pressure for separating H₂S of the feed stream, while the other three beds are working at lower pressure and high temperature for regeneration mode. On the other hand, if the company chooses to operate at the maximum flow rate ($Q = 0.420 \text{ m}^3/\text{s}$) with only one bed of 1.09 m diameter and 3.82 m of length, the bed saturation time should be about three times shorter, which would require adsorbent replacement and/or an early bed regeneration. The breakpoint time for the flow of $0.420 \text{ m}^3/\text{s}$ and only one bed would be 15.4 h. This value is very close to that reported in the literature for the removal of mercaptans in UPGN, around 18 h, as reported ([Khademi et al., 2015](#); [Qazvini and Fatemi, 2015](#); [Ahari et al., 2016](#); [Yousefi et al., 2017](#)), for gas streams with the same order of magnitude of contaminant concentration, and similar column diameters and bed lengths. In this case, one column is in operation while the other is maintained in regeneration. Therefore, by considering the operation of the adsorption unit at the maximum flow rate, the regeneration time or adsorbent bed replacement match the data reported in the literature, providing the desulphurization of the gas stream before its transportation through the pipeline to the onshore facility, avoiding S₈ formation and deposition problems.

The results found in the simulations showed the possibility of using equilibrium data to predict the operating conditions that occur in the gas pipeline. In addition, the breakthrough curves showed that zeolite 13× could be an alternative for the removal of H₂S from a gas stream even under high pressure. According to [Sigot et al. \(2016b\)](#), the adsorption of H₂S on the surface of zeolite 13× involves the dissolution and

dissociation of H₂S in the pores and its oxidation to elemental sulfur, which confirms that the presence of this contaminant is probably the source of S₈. Therefore, the removal by adsorption is an attractive technique to solve the problem of S₈ formation and its deposition in the pipelines.

4. Conclusions

In this work, the H₂S removal from gas streams was evaluated by performing a scale-up based on pilot scale data studies to predict natural gas transport under real pipeline conditions. Our study concluded that:

- ✓ Experimental data obtained under pilot-scale experimental conditions could be corrected through the fitting of the Sips isotherm model to predict the equilibrium data in diverse experimental conditions.
- ✓ Based on the fitted model to simulate equilibrium data for H₂S removal using zeolite 13×, a scale-up to the real pressure and temperature conditions of natural gas transport through pipelines was performed.
- ✓ It was possible to perform a numerical analysis of the influence of operating parameters for different bed configurations modifying the variables (bed length/diameter ratio, pressure, and temperature), and for a confidence level of 95%, only pressure was statistically significant.
- ✓ Optimization of the operational conditions was performed, and the amount adsorbed in the equilibrium increased from 3.71 to 4.70 mol/kg.
- ✓ The overall mass transfer coefficient was very close for different flow rates, which indicates that the velocity is not too relevant, and the main resistance to mass transfer is due to the internal solid diffusion.
- ✓ The bed saturation times were estimated, and the predicted values are in agreement with the data reported by the literature for real natural gas desulphurization processes in a well-known Natural Gas Processing Unit, confirming that the implementation of this process is possible.

Declaration of competing interest

The authors declare that they have no known competing financial interests or personal relationships that could have appeared to influence the work reported in this paper.

Acknowledgment

This study was financed in part by the Coordenação de Aperfeiçoamento de Pessoal de Nível Superior - Brasil (CAPES) - Finance Code 001.

Appendix A. Supplementary data

Supplementary data to this article can be found online at <https://doi.org/10.1016/j.jngse.2020.103693>.

Nomenclature list

a	Sorption coefficient
b_0	adsorption constant at infinite temperature
b_S	Isotherm Constant Sips model
C	H ₂ S concentration in the gas phase
c	Diffusion coefficient
C_0	H ₂ S feed concentration
d_a	Damping coefficient or mass coefficient
D_e	Effective diffusivity
D_g	Distribution coefficient
D_K	Knudsen diffusivity

D_L	Axial dispersion coefficient
D_m	Molecular diffusivity
d_p	Adsorbent particle diameter
e_a	Mass coefficient
f	Source term
k_g	External mass transfer coefficient
K_s	Overall mass transfer coefficient
l	Dimensionless distance from the bed entrance
L	Total bed depth
m_{ads}	Adsorbent mass
$MM_{gás}$	Molecular weight of the gas mixture
MM_{H_2S}	Molecular weight of the H ₂ S
MTZ	Mass Transfer Zone
n	Exponent isotherm model
P	Pressure
Pe	Peclet number
Q	Feed rate
q_0	Maximum value of q in equilibrium with C
q_m	Maximum adsorption capacity
q_{sat}	Amount adsorbed to saturation
q_u	Quantity adsorbed to breakpoint
Re	Reynolds number
r_{pore}	Porous radius
S	Dimensionless mass transfer coefficient
Sc	Schmidt number
Sh	Sherwood number
t	Time
T	Temperature
t_b	Breakpoint time
t_u	Useful time
u_1	Dimensionless concentration of H ₂ S in the gas phase
u_2	Dimensionless concentration of H ₂ S in solid phase
$V_{gás}$	Diffusion volume of the gas
V_{H_2S}	Diffusion volume of the H ₂ S
Z	Bed length

Greek letters

α	Conservative flux convection coefficient
β	Convection coefficient
γ	Conservative flux source term
ε	Bed void fraction
ε_p	Particle porosity
ρ_b	Bed bulk density
ρ_p	Particle density
τ	Dimensionless time
τ_p	Particle tortuosity
v	Interstitial velocity

Credit author statement

João Paulo Lobo dos Santos: Conceptualization; Data curation, Investigation and Writing - original draft. Ana Katerine de Carvalho Lima Lobato: Conceptualization and Methodology. Caetano Moraes: Supervision and Writing - review & editing. Acto de Lima Cunha: Methodology, Software and Validation. José Jailton Marques: Writing - review & editing, Luiz Carlos Lobato dos Santos: Project administration, Resources, Supervision and Writing - review & editing.

References

- Abdulredha, M.M., Hussain, S.A., Abdullah, L.C., 2020. Optimization of the demulsification of water in oil emulsion via non-ionic surfactant by the response surface methods. *J. Petrol. Sci. Eng.* 184, 106463.
- Aguilera, P.G., Ortiz, F.J.G., 2016. Prediction of fixed-bed breakthrough curves for H₂S adsorption from biogas: importance of axial dispersion for design. *Chem. Eng. J.* 289, 93–98.
- Ahari, J.S., Shafiee, Z., Mohammadbeigy, K., Pakseresht, S., Kakavand, M., Kolivand, M., 2016. Modeling and investigation of the operational parameters in the process of mercaptan and water removal from natural gas by adsorption on zeolite 13X. *Pet. & Coal* 58 (3), 307–320.
- Alami, I.A., Al-Haji, M.N., Al-Adel, S.I., 2012. Saudi aramco offshore sour gas production: elemental sulfur deposition mitigation. *Saudi aramco journal of technology*, p. 13. Arábia Saudita.
- Anerousis, J.P., Whitman, S.K., 1985. Iron Sponge: still a top option for sour gas sweetening. *Oil Gas J.* 18, 71–76.
- Castrillon, M.C., Moura, K.O., Alves, C.A., Bastos Neto, M., Azevedo, D.C.S., Hofmann, J., Möllmer, J., Einicke, W.D., Glaser, R., 2016. CO₂ and H₂S removal from CH₄-rich streams by adsorption on activated carbons modified with K₂CO₃, NaOH or Fe₂O₃. *Energy & Fuels*.30(11) 9596–9604.

- Coppola, G., Papurello, D., 2018. Biogas cleaning: activated carbon regeneration for H₂S removal. *Cleanroom Technol.* 1 (1), 40–57.
- Dantas, T.L.P., Luna, F.M.T., Silva Júnior, I.J., Torres, A.E.B., Azevedo, D.C.S., Rodrigues, A.E., Moreira, F.P.M., 2011. Modeling of the fixed-bed adsorption of carbon dioxide and a carbon dioxide-nitrogen mixture on zeolite 13X. *Braz. J. Chem. Eng.* 28, 533–544.
- Ezeakacha, C.P., Salehi, S., 2019. Experimental and statistical investigation of drilling fluid loss in porous media: Part 2 (Fractures). *J. Nat. Gas Sci. Eng.* 65, 257–266.
- Faiz, R., Al-Marzouqi, M., 2010. H₂S absorption via carbonate solution in membrane contactors: effect of species concentrations. *J. Membr. Sci.* 350, 200–210.
- Faramawy, S., Zaki, T., Zakr, A.A.E., 2016. Natural gas origin, composition, and processing: a review. *J. Nat. Gas Sci. Eng.* 34, 34–54.
- Geankoplis, C.J., 1993. *Transport Processes and Unit Operations*, third ed. Englewood Cliffs, New Jersey.
- Khademi, S., Anisi, H., Mirian, S., Yu, X., Sadighi, S., 2015. A mathematical model to design mercaptans removal unit (MRU) using real component lumping approach. *Pet. & Coal* 57 (6), 609–618.
- Kim, W., Yun, C., Jung, K.T., Park, S., Kim, S.H., 2012. Computer-aided scale-up of a packed-bed tubular reactor. *Comput. Chem. Eng.* 39, 96–104.
- Kimantas, C.L., Taylor, M.A., 2014. An effective solution for elemental sulfur deposition in natural gas systems. In: Presented at the American Filter and Separation Society Conference, Houston, Texas, USA.
- Ko, C.H., Song, H.I., Park, J.H., Han, S.S., Kim, J.N., 2007. Selective removal of sulfur compounds in city-gas by adsorbents. *Kor. J. Chem. Eng.* 24 (6), 1124–1127.
- Ko, D.D.K., Porter, J.F., Mackay, G., 2000. Film-pore diffusion of copper and cadmium ions onto bone char. *Water Res.* 35, 3876–3886.
- Liu, T., First, E.L., Fraque, Hasan M.M., Floudas, C.A., 2016. A multi-scale approach for the discovery of zeolites for hydrogen sulfide removal. *Comput. Chem. Eng.* 91, 206–218.
- Melo, D.M.A., Souza, J.R., Melo, M.A.F., Martinelli, A.E., Cachima, G.H.B., Cunha, J.D., 2006. Evaluation of the zirconium and zeolite materials as adsorbents to remove H₂S from natural gas. *Colloids Surf., A* 272, 32–36.
- Mirfendereski, M., Mohammadi, T., 2017. Investigation of H₂S and CO₂ removal from gas streams using hollow fiber membrane gas-liquid contactors. *Chem. Biochem. Eng. Q.* 31 (2), 139–144.
- Oliveira, L.H., Meneguim, J.G., Silva, E.A., Barros, M.A.S.D., Arroyo, P.A., Grava, W.M., Nascimento, J.F., 2014. Prediction of three component gas adsorption with IAST and Langmuir. *COBEQ Congresso Brasileiro de Engenharia Química, Florianópolis- SC* 1–8.
- Ortiz, F.J.G., Aguilera, P.G., Ollero, P., 2014. Modeling and simulation of the adsorption of biogas hydrogen sulfide on treated sewage-sludge. *Chem. Eng. J.* 253, 305–315.
- Pack, D.J., Parks, D.W., Chesnoy, A.B., 2012. Gas pipeline preferential site selection occurrence for elemental sulphur & other particle matter formation & deposition. *J. Petrol. Sci. Eng.* 94–95, 12–18.
- Possa, R.D., Sousa, J.F., Oliveira, J.A., Nascimento, P.F.P., Lima, M.T.A., Brandão, I.B., Bezerra, M.B.D., 2018. Dynamic adsorption of H₂S in a fixed bed of sewage sludge pyrolysis char. *Braz. J. Pet. Gas.* 12 (2), 77–90.
- Qazvini, O.T., Fatemi, S., 2015. Modeling and simulation pressure-temperature swing adsorption process to remove mercaptan from humid natural gas; a commercial case study. *Separ. Purif. Technol.* 139, 88–103.
- Ratnasamy, C., Wagner, J.P., Spivey, S., Weston, E., 2012. Removal of sulfur compounds from natural gas for fuel cell applications using a sequential bed system. *Catal. Today* 198, 233–238.
- Rezakazemi, M., Niazi, Z., Mirfendereski, M., Shiraziam, S., Mohammadi, T., Pak, A., 2011. CFD simulation of natural gas sweetening in a gas-liquid hollow-fiber membrane contactor. *Chem. Eng. J.* 168 (3), 1217–1226.
- Ryzhikov, A., Hulea, V., Tichit, D., Leroi, C., Anglerot, D., Coq, B., Trens, P., 2011. Methyl mercaptan and carbonyl sulfide traces removal through adsorption and catalysis on zeolites and layered double hydroxides. *Appl. Catal., A* 397, 218–224.
- Santos, J.P.L., Cunha, A.L., Lobato, A.K.C.L., Moraes, C., Severo Junior, J.B., Santos, L.C.L., 2018. Modeling and simulation of the desulfurization of a sour gas streams by adsorption: influence of the isotherm model. *Chem. Ind. Chem. Eng. Q.* 25 (1), 77–87.
- Santos, J.P.L., Lima Lobato, A.K.C., Moraes, C., Severo Júnior, J.B., Marques, J.J., Santos, L.C.L., 2019. Evaluation of the influence of operating parameters in the modeling and simulation of sour gas stream desulfurization by adsorption. *Energy Fuels* 33, 1673–1681.
- Santos, J.P.L., Lobato, A.K.C.L., Moraes, C., Santos, L.C.L., 2015. Determination of elemental sulfur deposition rates for different natural gas compositions. *J. Petrol. Sci. Eng.* 135, 461–465.
- Santos, J.P.L., Lobato, A.K.C.L., Moraes, C., Cunha, A.L., Silva, G.F., Santos, L.C.L., 2016. Comparison of different processes for preventing deposition of elemental sulfur in natural gas pipelines: a review. *J. Nat. Gas Sci. Eng.* 32, 364–372.
- Sekhvatjou, M.S., Moradi, R., HosseiniAlhashemi, A., TaghniaHejabi, A., 2014. A new method for sulfur components removal from sour gas through application of zinc and iron oxides nanoparticles. *Int. J. Environ. Res.* 8 (2), 273–278.
- Sigot, L., Obis, M.F., Benbelkacem, H., Germain, P., Ducom, G., 2016a. Comparing the performance of a 13X zeolite and na impregnated activated carbon for H₂S removal from biogas to fuel an SOFC: influence of water. *Int. J. Hydrogen Energy* 1–9.
- Sigot, L., Ducom, G., Germain, P., 2016b. Adsorption of hydrogen sulfide (H₂S) on zeolite (Z): retention mechanism. *Chem. Eng. J.* 287, 47–53.
- Svedberg, U.G., 1979. Simulation and scale-up of adsorption columns. *Comput. Chem. Eng.* 3, 549–551.
- Teles, V.H.B., Silva, J.D., 2015. Pressure swing adsorption technology using 5A zeolite for the removal of H₂S in the fixed bed reactor. *Chem. Eng. Trans.* 43, 1111–1116.
- Vijayaraghavan, K., Jegan, J., Palanivelevu, K., Velan, M., 2005. Biosorption of copper, cobalt and nickel by marine green *Alga Ulva reticulata* in a packed column. *Chemosphere* 60, 419–426.
- Wang, J., Ju, F., Han, L., Qin, H., Hu, Y., Chang, L., Bao, W., 2015. Effect of activated carbon supports on removing H₂S from coal-based gases using Mn-based sorbents. *Energy & Fuels* 29(2) 488–495.
- Watabe, T., Yogo, K., 2013. Isotherms and isosteric heats of adsorption for CO₂ in amine-functionalized mesoporous silicas. *Sep. Purif. Technol.* 120, 20–23.
- Wynnyk, K.G., Hojjati, B., Pirzadeh, P., Marrioti, R.A., 2017. High-pressure sour gas adsorption on zeolite 4A. *Adsorption* 23 (1), 149–162.
- Xu, Z., Cai, J., Pan, B., 2013. Mathematically modeling fixed-bed adsorption in aqueous systems. *Appl. Phys. Eng* 14 (3), 155–175.
- Yousefi, H., Mehrpooya, M., Naeiji, E., 2017. Modeling and optimization of currently in operation natural gas desulfurization process using adsorption separation method. *Chem. Eng. Process. Process Intensif.* 120, 220–233.
- Zhou, F., Hongchuan, L., Jianyi, L., Xu, O.Y., Liuli, L., 2013. The elemental sulfur deposition and its corrosion in high sulfur gas fields. *Nat. Gas Ind.* 33, 102–109.
- Zulkefli, N.N., Masdar, M.S., Isahac, W.R.W., Jahim, J., Majlam, E.H., Rejab, S.A.M., Lye, C.C., 2017. Mathematical modelling and simulation on the adsorption of hydrogen sulfide (H₂S) gas. *IOP conf. Ser.: mater. Sci. Eng.* 206, 012069.
- Zulkefli, N.N., Masdar, M.S., Isahac, W.R.W., Jahim, J., Rejab, S.A.M., Lye, C.C., 2019. Removal of hydrogen sulfide from a biogas mimic by using impregnated activated carbon adsorbent. *PLoS One* 14 (2), e0211713.